Preparation and characterization of metal-organic framework/microencapsulated phase change material composites for indoor hygrothermal control

Journal of Building Engineering 31 (2020) 101345

Contents lists available at ScienceDirect

Journal of Building Engineering

journal homepage: http://www.elsevier.com/locate/jobe

Preparation and characterization of metal-organic framework /microencapsulated phase change material composites for indoor hygrothermal control

Pumin Hou, Menghao Qin *, Shuqing Cui, Kan Zu

Department of Civil Engineering, Technical University of Denmark, Lyngby, 2800, Denmark

ARTICLE INFO

Keywords:
Microencapsulated phase change material
MIL-100(Fe)
Thermal and humidity buffering
Hygrothermal simulation

ABSTRACT

Building materials with high thermal and hygric inertia can moderate the fluctuation of indoor temperature and relative humidity, and thus can improve the indoor thermal comfort and reduce the building energy consumption passively. In this study, a novel hygrothermal control material was prepared based on Metal-Organic Frameworks (MOFs) and microencapsulated phase change material (MicroPCM). The new MOF/MicroPCM composite has a dual functionality of adsorption and desorption of both heat and moisture, can offer an accurate passive control of the indoor hygrothermal environment. N-octadecane was encapsulated by polymethylmetracrylate (PMMA) as MicroPCM for the thermal buffering. MIL-100(Fe) was prepared by the hydrothermal reaction method as the humidity buffering material. A series of hygrothermal control composite materials were obtained by grinding MicroPCM and MIL-100(Fe). Physicochemical properties of the synthesized materials were characterized by SEM, TEM, XRD, FTIR, N_2 physisorption, Water vapor sorption isotherm, DSC and TGA techniques. Hygrothermal properties of the composites were analyzed in comparison to pure MicroPCM and MIL-100(Fe). The thermal and humidity buffering behavior of the composites containing 50% MicroPCM was analyzed by numerical simulations. The results show that the composites possess an excellent thermal and humidity buffer capacity, which can be used for building energy-saving and improving thermal comfort.

1. Introduction

The building sector accounts for 40% of global energy which is mainly provided by fossil fuel and corresponding to over one-third of carbon dioxide emissions [1,2]. Reducing building energy consumption plays an active part in mitigating global problems such as energy fuel depletion, environmental pollution, and global warming. Passive design method is an effective method to reduce building energy consumption and improve indoor thermal comfort [3,4].

Among various passive design methods, the integration of phase change material with the building envelope has been widely studied to improve the thermal inertia and reduce temperature fluctuation [5–7]. However, this solution has little effect on the regulation of relative humidity, which also has a significant impact on building energy consumption and occupants' comfort [8,9]. Hygroscopic porous materials can automatically adjust the relative humidity of the indoor environment rely solely on their own moisture absorption and desorption properties [10].

Normally it is difficult to regulate both temperature and humidity at the same time by a single PCM or porous material. Recently, some researches have combined microencapsulated PCMs with conventional porous materials (e.g., diatomite, vesuvianite, sepiolite, and zeolite, etc.) to simultaneously regulate temperature and humidity in the building [11–13]. These hygrothermal materials show a promising energy saving potential and the maximal energy-saving rate could be up to 19.57% [14]. However, the conventional hygroscopic materials are suffering from low moisture absorption capacity and high requirements for desorption (e.g. high regeneration temperature, etc.) [15]. In order to make the hygrothermal material have a certain moisture absorption capacity by simple physical mixing as mentioned in previous research, the porous material has to occupy a considerable proportion, which will make the enthalpy of the composite materials greatly reduced. Another disadvantage is that the pore size distribution of the conventional porous materials is irregular and the corresponding water adsorption isotherms do not satisfy the V-type adsorption curve, which is considered to be the most beneficial for thermal comfort in buildings [16].

* Corresponding author.
E-mail address: menqin@byg.dtu.dk (M. Qin).

https://doi.org/10.1016/j.jobe.2020.101345
Received 2 December 2019; Received in revised form 8 March 2020; Accepted 8 March 2020
Available online 10 March 2020

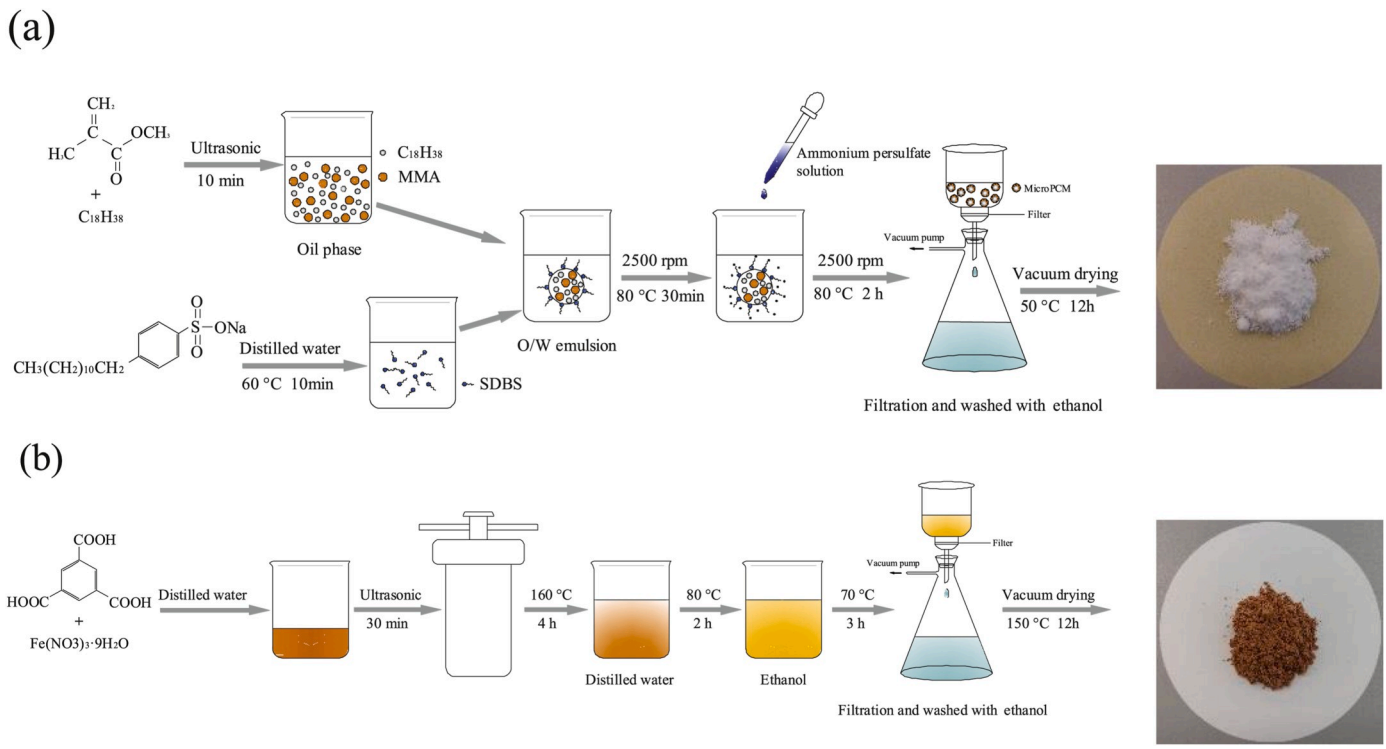

Fig. 1. Schematic representation of the fabrication procedure of (a) MicroPCM and (b) MIL-100(Fe).

Metal-organic framework (MOF) is a new kind of porous crystalline material with a periodic network structure formed by self-assembly of inorganic metal nodes and organic linkers [17,18]. MOF is becoming a promising alternative for moisture adsorption due to its high specific surface area, permanent porosity, tunable crystalline structure, and organic functionality [19–22]. MIL-100(Fe) as one of the major crucial MOF that possesses high water uptake capacity, hydrothermal and cycle stability [23]. In addition, the main constituent element iron atom is non-toxic, widely sourced, inexpensive, and environmentally friendly [24], making MIL-100(Fe) a priority for this work.

In this paper, a series of MIL-100(Fe)/MicroPCM composites were prepared and studied for temperature and humidity control. Firstly, the MicroPCM and MIL-100(Fe) were prepared by interfacial polymerization [25] and hydrothermal reaction method [24] respectively. Then two ingredients mixed sufficiently by gridding. The homogeneous composites were characterized by SEM, TEM, N_2 adsorption, XRD, FTIR, Water Isotherm, DSC and TGA techniques. Finally, the thermal and humidity buffering behavior of the composites is evaluated by numerical simulations.

2. Materials preparation

2.1. Raw materials

Methyl methacrylate (MMA), n-octadecane, Sodium dodecyl benzene sulfonate (SDBS) and ammonium persulfate were offered by Sinopharm chemical. Ferric sulfate nonahydrate ($Fe(NO_3)_3{\cdot}9H_2O$) and Benzene-1,3,5-tricarboxylic acid (H_3BTC) were purchased from Sigma-Aldrich. All chemicals used in the experiment are analytical reagents without further purification.

2.2. Synthesis of MicroPCM

MicroPCMs were prepared by encapsulating the core material n-octadecane with PMMA using interfacial polymerization. The schematic production process is illustrated in Fig. 1(a). 21 g n-octadecane and 9 g MMA were mixed by ultrasonic for preparing the oil phase. 3% SDBS was added into 30 g distilled water and agitated with 2500 rpm in a flask at 60 °C for preparing the water phase. Then the oil phase was added to the water phase and improved the temperature to 80 °C and stirred for 30 min to prepare the O/W emulsion. Finally, 1% ammonium persulfate solution (0.13 g/ml) of MMA quality was dropwise added into the above emulsion as initiator and maintained the temperature and stirring rate until the end of the polymerization after 2 h. The products were covered by filtration and washed with distilled water 3 times. The white powders were obtained by vacuum drying at 50 °C for 12 h.

2.3. Synthesis of MIL-100(Fe)

MIL-100(Fe) was prepared by the hydrothermal reaction method. The schematic production process is illustrated in Fig. 1(b). 5 g Fe $(NO_3)_3{\cdot}9H_2O$ and 1.73 g H_3BTC (molar ratio 1.5:1) were dissolved in 1 g distilled water by sonication for 10 min. Then the solution was transferred to a 100 ml Teflon-lined autoclave and heated in an oven at 160 °C for 4 h. The obtained reaction product purified using 100 ml distilled water at 80 °C for 2 h and 100 ml ethanol at 70 °C for 3 h. The products were covered by filtration at each purification step and washed with ethanol 3 times. Finally, claybank solid was obtained by vacuum drying at 150 °C for 12 h.

2.4. Synthesis of MIL-100(Fe)/MicroPCM composites

MIL-100(Fe)/MicroPCM composites were obtained by hand gridding. Firstly, the MicroPCM and MIL-100(Fe) were dried in a vacuum oven at 50 and 70 °C for 24 h, respectively. Then different ratios of MIL-100 (Fe) and MicroPCM were mixed and ground in ambient atmosphere at least 5 min until homogeneous. Finally, a series of composites containing different proportions of MIL-100(Fe) and MicroPCM were obtained.

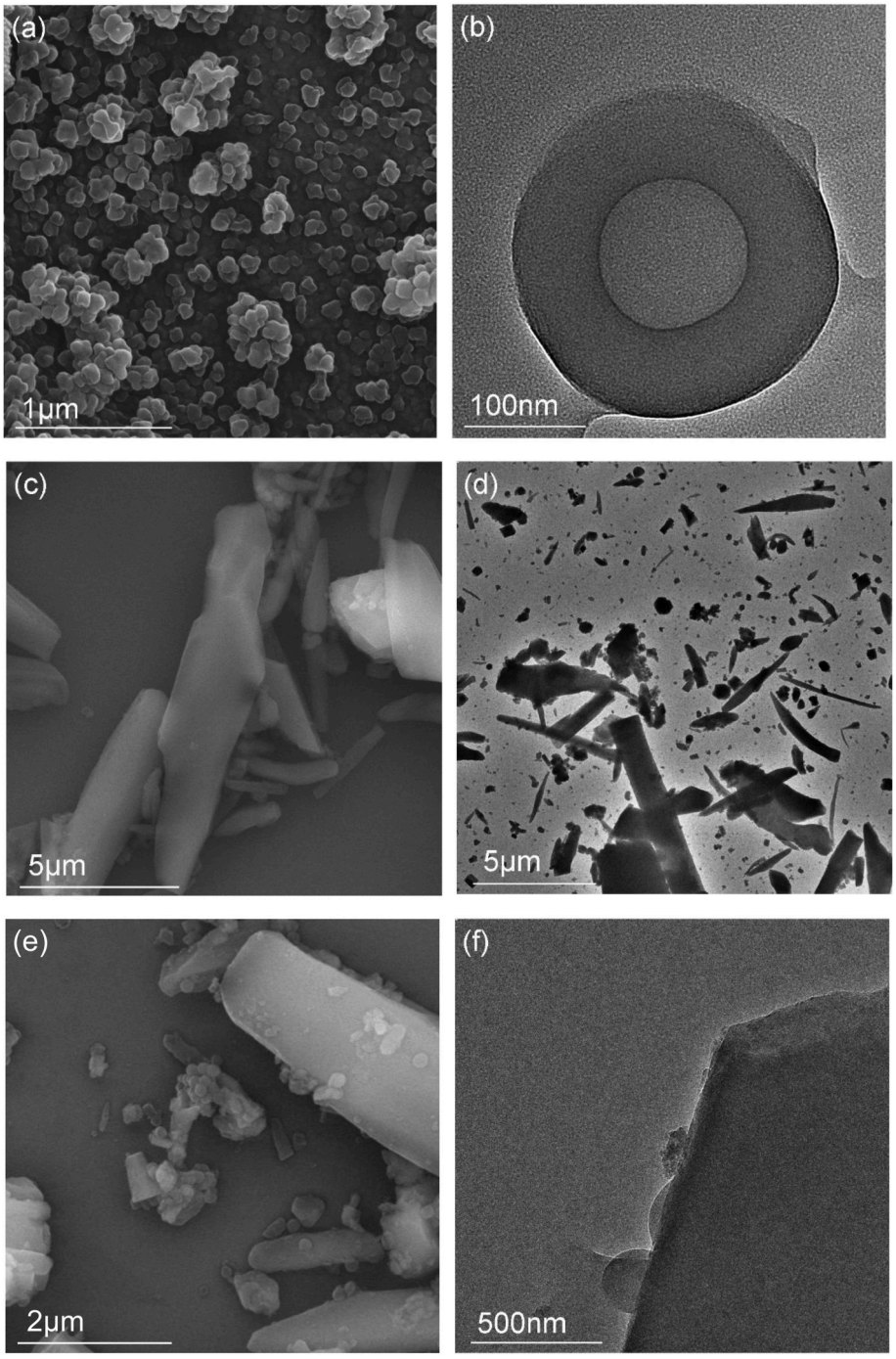

Fig. 2. SEM and TEM image of MicroPCM (a and b), MIL-100(Fe) (c and d) and MIL-100(Fe)/MicroPCM (e and f).

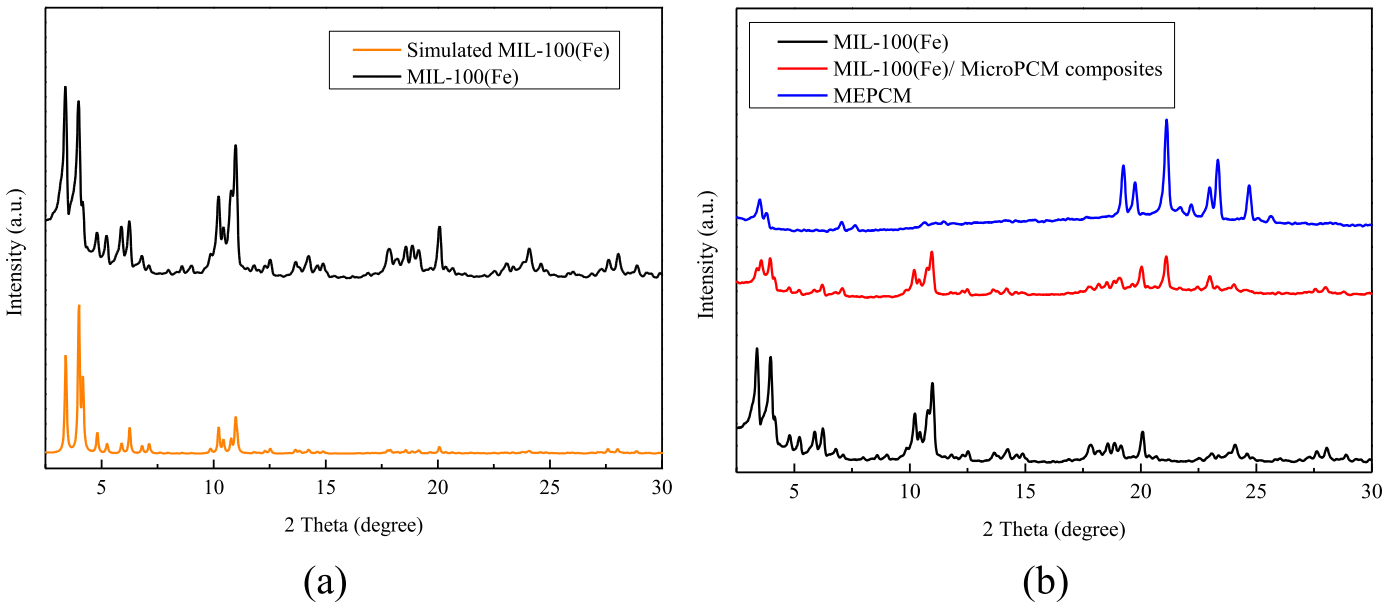

Fig. 3. XRD Patterns of simulated and as-synthesized MIL-100(Fe), MicroPCM and MIL-100(Fe)/MicroPCM composites.

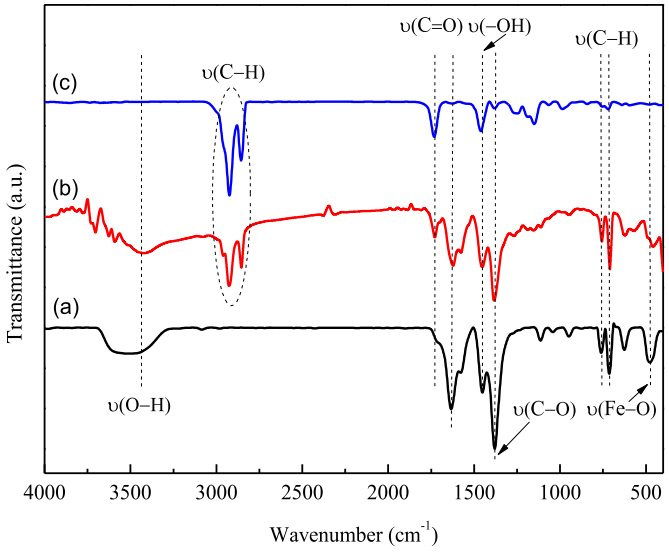

Fig. 4. FTIR spectra of as synthesized (a)MIL-100(Fe), (b)MicroPCM and (c) MIL-100(Fe)/MicroPCM composites.

3. Characterization

Morphologies of the materials were investigated by scanning electron microscope (SEM; FEI Nova Nano SEM 450) at an accelerating voltage of 15 kV. Detail structures of the microcapsules were researched on a transmission electron microscopy (TEM; FEI Tecnai F30) at 200 kV. N_2 sorption isotherms were obtained on an ASAP 2020 micromeritics at −196 °C. Water sorption isotherms were measured by a dynamic vapor sorption (DVS intrinsic; SMS) instrument. Powder X-ray diffraction (XRD) patterns were recorded on a diffractometer (Rigaku Smartlab9) from 2 to 90°. Fourier transform infrared (FTIR) spectra were measured on a spectrometer (Bruker Verte-80). Differential scanning calorimeter (DSC) curves were obtained by TA Q200 from −10 °C to 50 °C with the heating rate of 10 °C/min under N_2 atmosphere. The thermal stability was tested by thermal gravimetric analyzer (TGA; TA Q50) from ambient temperature to 600 °C with the heating rate 20 °C/min under N_2 atmosphere.

3.1. Microscopic morphology and chemical characterization

SEM image of the MicroPCM is shown in Fig. 2(a). It can be observed that the synthesized microcapsules have relatively uniform sizes in hundreds of nanometers. As illustrated in the TEM image (Fig. 2 (b)) of MicroPCM, the microsphere is composed of n-octadecane core and PMMA shell, clearly exhibiting a core-shell structure. Fig. 2(c) and (d) present the SEM and TEM pictures of MIL-100(Fe), it is obvious that the MIL-100(Fe) is mainly composed of stick-like crystals. As shown in Fig. 2 (e) and (f), MicroPCM and MIL-100(Fe) were mixed, and some of the MicroPCM is adsorbed on the surface of the MIL-100(Fe).

XRD patterns of as-synthesized MIL-100(Fe) are presented in Fig. 3 (a). In order to facilitate comparison, the XRD patterns of the simulated data is also shown in Fig. 3(a). Diffraction peaks of MIL-100(Fe) synthesized in this work at 2θ values of 3.4, 4.0, 5.2, 11.0, 14.2, 18.2, 27.6° are consistent with the simulated one from crystal structure data [26]. The XRD patterns of MIL-100(Fe), MicroPCM and MIL-100 (Fe)/MicroPCM composite mixtures were collected and presented in Fig. 3 (b). Though the intensities of the diffraction peaks of composite mixtures attenuated a lot, all peaks in the composite mixtures curve corresponding to the peaks in MIL-100(Fe) and MicroPCM, indicating that two substances still retain good crystallinity after grinding mixing.

In order to get the chemical structures and compositions of the materials, the MIL-100(Fe), MicroPCM and MIL-100(Fe)/MicroPCM composites were studied by FTIR spectra and the results are shown in Fig. 4. FTIR spectra of as-synthesized MIL-100(Fe) shown in Fig. 4 is similar to the previous research [27,28], which further confirmed that the MIL-100(Fe) was synthesized successfully. It can be observed that the MIL-100(Fe) has a higher purity due to the disappearance of the C═O stretching vibration around 1714 cm^{-1}, which usually belongs to the residual H_3BTC over from reaction. Compared three spectra curves, the peak at 3400 cm^{-1} due to O–H corresponding water can only be found in MIL-100(Fe) and composites, which means that the MicroPCM is extremely hydrophobic. FTIR spectra reveal additional bands in the MIL-100(Fe)/MicroPCM composites corresponding to n-octadecane at 2924 and 2856 cm^{-1} attributed to the alkyl C–H stretching vibration of $–CH_2$ and-CH_3. Besides, the peak at1732 cm^{-1} denote C═O stretching vibrations of the ester group, which acted as a packaging material for capsuling phase change materials. The peak at 1622 cm^{-1} is attributed to the carboxylate groups, which provides interaction between COOH and Fe ion [29]. While the bands at 1452 cm^{-1} and 1381 cm^{-1} are

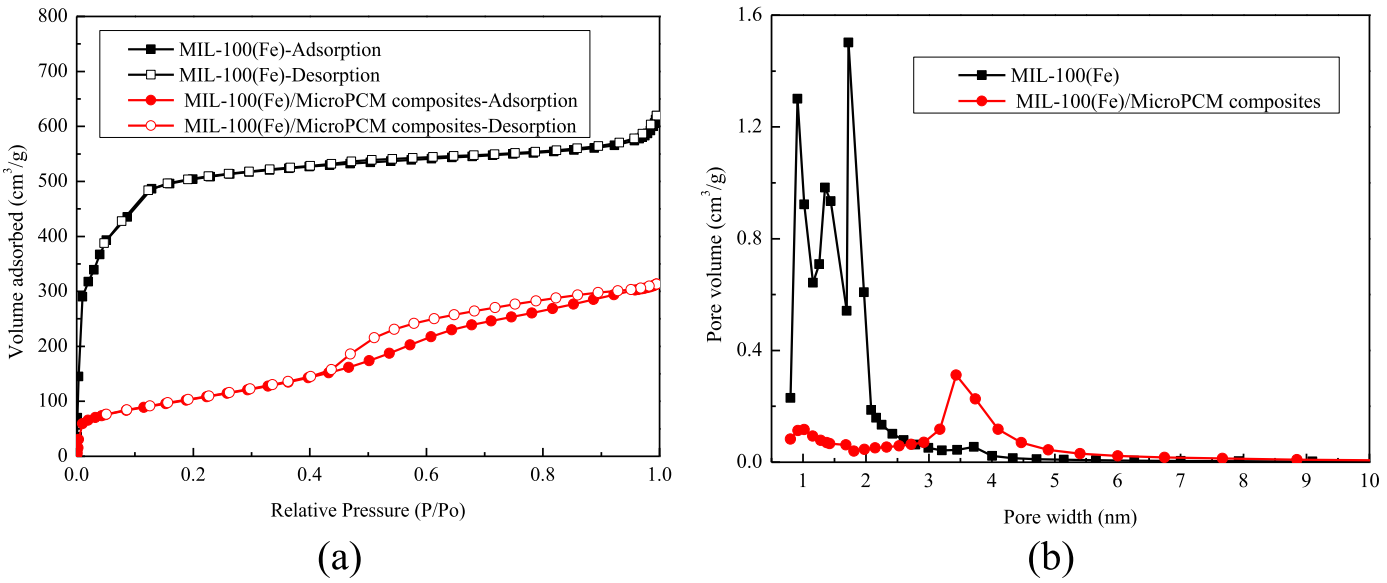

Fig. 5. (a) N_2 adsorption-desorption isotherms and (b) pore size distributions of MIL-100(Fe) and composites containing 50% MicroPCM.

mainly due to the symmetric –COOH group. Another two peaks at 760 and 714 cm^{-1} mainly due to C–H bending vibrations of benzene. The peak at 476 cm^{-1} stretching vibrations is caused by Fe–O. By comparing three FTIR spectra curves in Fig. 4, it can be seen that the curve (b) contained all vibration peaks occurred in the curve (a) and (c), which confirms that no chemical reaction occurred during the mixing process of MIL-100(Fe) and MicroPCM.

3.2. Sorption isotherms

Fig. 5(a) presents the N_2 adsorption-desorption isotherms of MIL-100 (Fe), MicroPCM and composites containing 50% MicroPCM. The Brunauer-Emmett-Teller (BET) specific surface area and total pore volume of MIL-100(Fe) and composites containing 50% MIL-100(Fe) is 1672 and 377 m^2/g, 0.93 and 0.49 cm^3/g, respectively. Both the two values of the composites are less than pure MIL-100(Fe), which is primarily due to the addition of nonporous MicroPCM. Fig. 5(b) shows the pore size distributions of MIL-100(Fe) and composites containing 50% MicroPCM. It was revealed that the pore size distribution of MIL-100(Fe) changed a lot after being ground with MicroPCM. The pore size of MIL-100(Fe) dominates at 0.9, 1.4 and 1.7 nm, while the pore size of composites containing 50% MIL-100(Fe) is mainly concentrated around 3.4 nm.

Water adsorption isotherms of MIL-100(Fe), MicroPCM and composites with varying content of MicroPCM were achieved by changing the relative humidity from 0 to 95% at 25 °C, the results were shown in Fig. 6. The relative humidity gradient during the test was 10% while the last step was 5%. When the mass change of the sample in each stage was less than 0.001%·min^{-1}, it was considered that the adsorption reached equilibrium at this stage and automatically entered the next stage. As presented in Fig. 6(a), the water adsorption isotherm of MIL-100(Fe) rises significantly from 20% to 50%, then increases slowly over the relative humidity, has the characteristic of "S" type. While the MicroPCM shows linear shape. The water uptake of MIL-100(Fe) at RH = 95% is 57.75%, which indicates that MIL-100 (Fe) as a moisture buffer material shows great potential in building energy-saving applications over traditional materials. The water uptake of MicroPCM is 0.85%, which again confirms its hydrophobicity. According to Fig. 6(b)–(d), the water uptake of composites was decreased with increasing the MicroPCM proportion. And the composites containing 30%, 50% and 70% MicroPCM reduced to 30.27%, 24.16% and 15.76%, respectively. Besides, the adsorption curve changed dramatically by adding MicroPCM. The trigger point of steep adsorption of MIL-100(Fe) moved from 20% RH to 70% RH. This is caused by the pore size change of MIL-100 (Fe). Besides, the trigger point of steep desorption moved from 40% to 70%, which means the composites are easier to desorb than the pure MIL-100(Fe). Compared the difference of water adsorption isotherm between pure MIL-100(Fe) and MIL-100(Fe)/MicroPCM composites, it can be found that the step (between 30% and 40% RH) caused by polymodal pore size distribution is disappeared as the percentage of MicroPCM increased to 50%. This can be confirmed from the pore size distribution of the composites above.

As shown in Fig. 6(b)–(d), the hysteresis loop between the sorption and desorption curves of composites is wider than pure MIL-100(Fe). Fig. 7 shows detail hysteresis data of MIL-100(Fe), MicroPCM and the composites at different relative humidity. It can be observed that the maximum hysteresis of pure MIL-100(Fe) and composites occurred at 40% and 70%, respectively. And the maximum value shows different degrees of reduction as the proportion of MicroPCM increased. This may be caused by two reasons. On the one hand, the addition of nonporous MicroPCM leads to the reduction of the water uptake. On the other hand, the PMMA-encapsulated MicroPCM increased the hydrophobicity of the composites.

3.3. Thermal properties

DSC curves of MIL-100(Fe), MicroPCM and MIL-100(Fe)/MicroPCM composites are presented in Fig. 8 and corresponding detailed thermal properties are listed in Table 1. As shown in Fig. 8 that all samples showed a single endothermic peak except for pure MIL-100(Fe), indicating that MIL-100 (Fe) has no phase transition during the test temperature range and the addition of MIL-100(Fe) does not change the crystallization form of MicroPCM. As shown in Table 1, both of the melting temperature (onset temperature) and peak temperature of MIL-100(Fe)/MicroPCM composites were reduced in various degrees compared with pure MicroPCM, which may be caused by the surface tension, capillary action and intermolecular force between the nanoparticles. The enthalpy value reduced rapidly as the proportion of MIL-100(Fe) increased. This is because both MicroPCM and MIL-100(Fe) were dried sufficiently before grinding. The MIL-100(Fe)/MicroPCM composites would adsorb moisture during grinding and the period before the DSC testing, which directly increased the weight of MIL-100 (Fe) and decreased the relative proportion of MicroPCM.

The thermal stability of the composites with varying content of MIL-

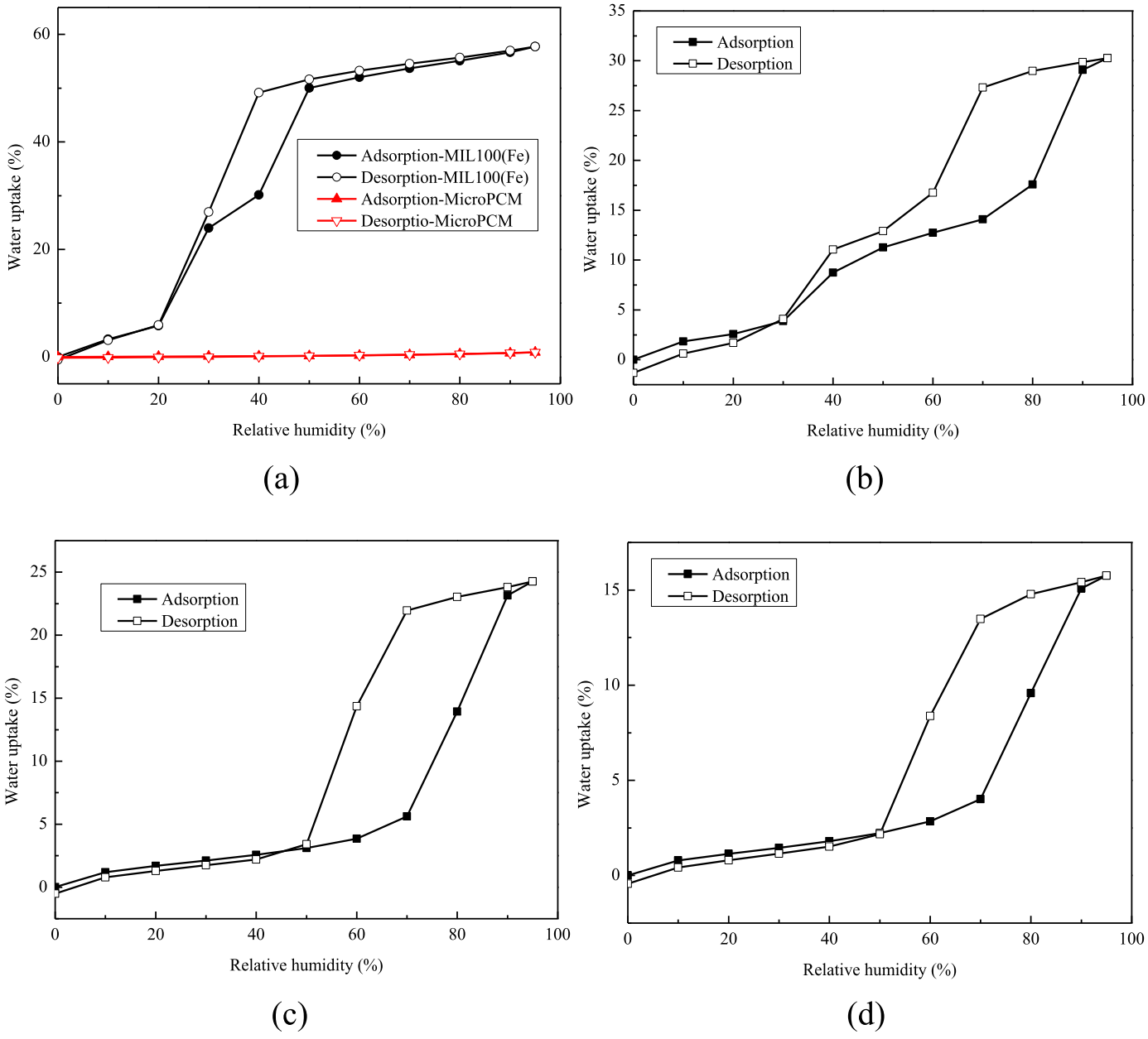

Fig. 6. Water adsorption isotherms of (a) MIL-100(Fe) and MicroPCM and (b)–(d) MIL-100(Fe)/MicroPCM composites containing 30%, 50% and 70% MicroPCM.

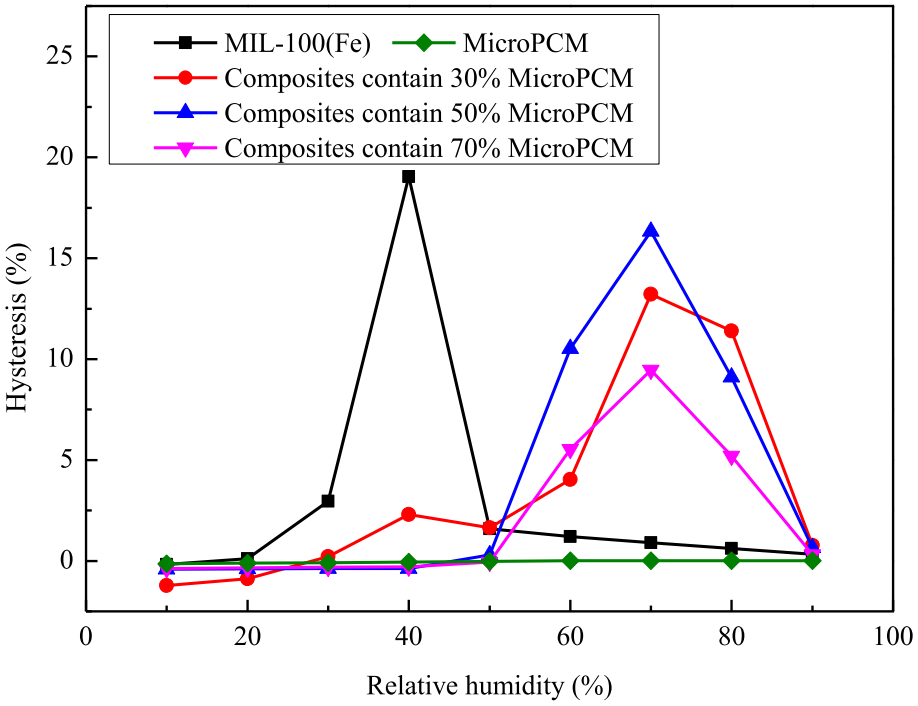

Fig. 7. Hysteresis of MIL-100(Fe), MicroPCM and the composites.

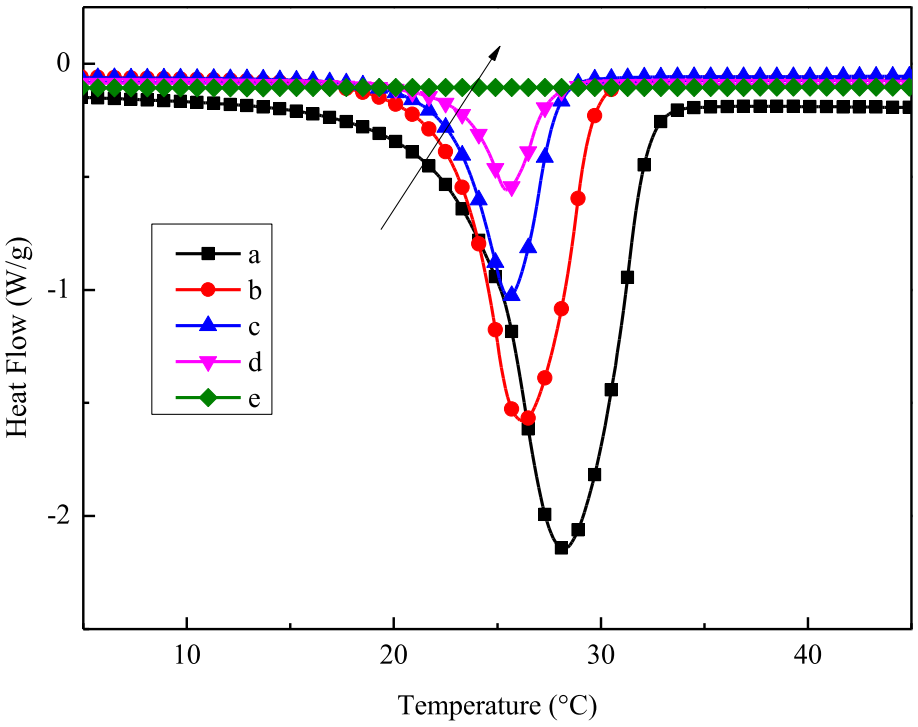

Fig. 8. DSC curves of MIL-100(Fe)/MicroPCM composites (a)–(e): containing 100%, 70%, 50%, 30%, 0% MicroPCM.

100(Fe) and MicroPCM was measured by a TG analyzer. Fig. 9 demonstrates the TG results of the composites and Table 2 shows the degradation data including initial decomposition temperature and residual mass. The weight loss process of MIL-100(Fe) is roughly divided into three stages [30]. The initial weight loss (about 14 wt%) bellow 100 °C due to the desorption of free water. The second step (about 13 wt%) from 100 to 300 °C is ascribed to the loss of bonded water. The last step (about 31 wt%) occurred at the temperature between 300 and 520 °C is caused by the decomposition of trimesic acid. The degradation of MicroPCM has three steps and the initial decomposition temperature starts at roughly 192 °C and completely loses its weight at around 465 °C. At the first step, the mass drop sharply between 105 and 237 °C due to the evaporation of octadecane, which is comprised of linear alkane with low thermal decomposition temperature [31]. The second and third step was ascribed to the monomer evolution and the random bond scission of the PMMA shell, respectively [32]. The weight loss rate of the

Table 1
Thermal properties of composites with varying content of MIL-100(Fe) and MicroPCM.

Sample	MicroPCM contents (%)	Melting temperature (°C)	Peak temperature	Enthalpy (J/g)
a	100	24.05	28.16	144.20
b	70	22.90	26.27	90.76
c	50	22.67	25.66	44.78
d	30	23.27	25.43	18.45
e	0	–	–	0

composites is improved with the increase of the content of MIL-100(Fe) at the beginning. Along with the rise of temperature, the curves show a reverse trend. This is because that the weight loss at lower temperatures is mainly caused by evaporation of water, while the composite with higher MIL-100(Fe) can adsorb more water vapor. Once the temperature rises to the thermal decomposition point of octadecane, the weight loss rate of composites with lower MIL-100(Fe) content will quickly exceed others. Finally, the composites with lower MIL-100(Fe) have less residual mass at 600 °C.

4. Hygrothermal buffering behavior of MIL-100(Fe)/MicroPCM composites

In order to evaluate the effect of MIL-100(Fe)/MicroPCM composites on the indoor climate of building. Hygrothermal buffering behavior of the composites containing 50% MicroPCM was analyzed by numerical simulation [33] using software WUFI Plus. A single-room model was built based on the case 600 from the International Energy Agency (IEA) ECBCS Annex 21 [34]. Detail dimensions of the building are shown in Fig. 10. The selected building faces south with a floor area of 48 m^2 and volume of 129.6 m^3. Two south-facing double-glazed windows with dimensions of 2 m × 3 m. The properties of the materials used in different layers are shown in Table 3. It should be noted that the underfloor insulation assumed with the minimum density and specific heat. The light weight building was assumed in Rome with a typical Mediterranean climate. The mechanical ventilation rate is 0.5 ACH for the whole day. The case 600 model with hygrothermal buffering material installed 2 cm thickness composites containing 50% MicroPCM on the internal wall. For comparison, the reference room added 2 cm thickness plasterboard.

Figs. 11–13 show the fluctuation in indoor temperature and humidity for a typical summer week in July. Compared with the reference room, the room with MIL-100(Fe)/MicroPCM composites has a significant reduction of periodic fluctuations in temperature. This is mainly due to the thermal storage of phase change material. It can be seen from Figs. 12 and 13, both of the relative and absolute humidity have smaller amplitudes for room with MIL-100(Fe)/MicroPCM composites. This is because that the composites show good buffering capacity that can absorb and release moisture.

Further analysis found that the greater the temperature and relative humidity difference between day and night, the great the advantages of MIL-100(Fe)/MicroPCM composites for indoor hygrothermal control. For example, the temperature difference between day and night on July 1 was 9 °C and the relative humidity difference was 39% RH. For the room with MIL-100(Fe)/MicroPCM composites as enclosure, the temperature and moisture content at 2:00 p.m. were 30.5 °C and 16.38 g/kg, respectively. While for the reference room with plaster, the temperature and moisture content were 33.6 °C and 18.0 g/kg, respectively. Conclusions can be drawn that the MIL-100(Fe)/MicroPCM composites can make full use of the temperature and humidity gradient between day and night and significantly reduce the daytime peak temperature and moisture content.

Table 2
TG data of composites with varying content of MIL-100(Fe) and MicroPCM.

Sample	MicroPCM contents (%)	Initial decomposition temperature (°C)	Residual mass at 600 °C (%)
a	100	192.2	0
b	70	168.9	26.7
c	50	168.4	34.2
d	30	49.9	35.3
e	0	49.0	40.5

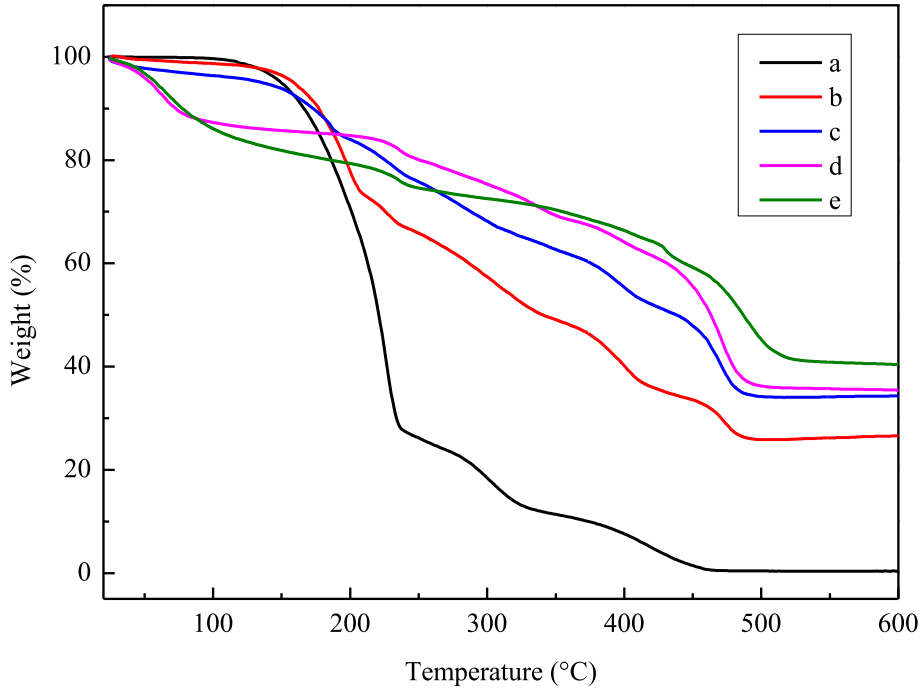

Fig. 9. TG curves of MIL-100(Fe)/MicroPCM composites (a)–(e): containing 100%, 70%, 50%, 30%, 0% MicroPCM.

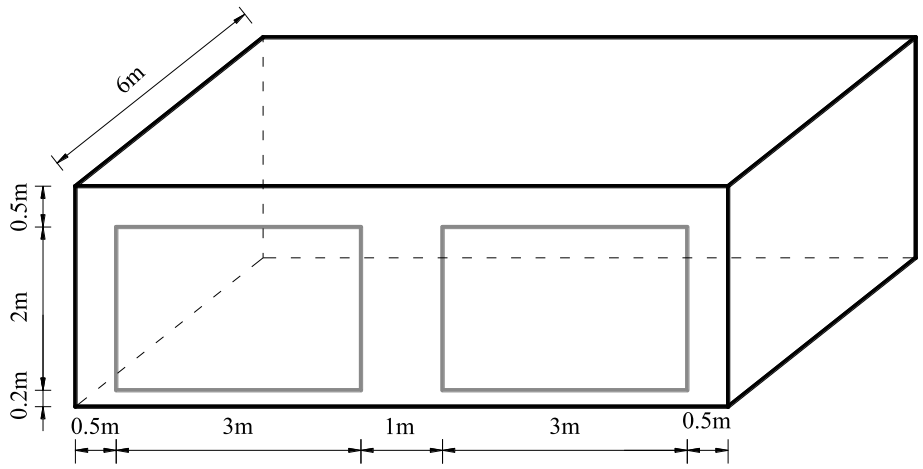

Fig. 10. The BESTEST lightweight case building.

Table 3
Properties of the envelop materials.

Construction	Material	Thickness (m)	Dry density (kg/m^3)	Porosity (m^3/m^3)	Specific heat capacity (J/kg·K)	Thermal conductivity (W/m·K)	U (W/m^2·K)	Vapor diffusion resistance (–)
Wall (outside to inside)	Ext surf coef						29.3	
	Wood siding	0.009	530	0.666	900	0.14	15.556	53.1
	Fibreglass quilt	0.066	12	0.99	840	0.04	0.606	1.3
	Plasterboard	0.012	950	0.61	840	0.16	13.333	9
	Int Surf Coef						8.29	
Floor (outside to inside)	Insulation	1.003	1	0.01	1	0.04	0.04	500
	Timber flooring	0.025	650	0.47	1200	0.14	5.6	200
	Int Surf Coef						8.29	
Roof (outside to inside)	Ext surf coef						29.3	
	Roofdeck	0.019	530	0.1	900	0.14	7.368	13
	Fiberglass quilt	0.1118	12	0.99	840	0.04	0.358	1.3
	Plasterboard	0.01	950	0.61	840	0.16	16	9
	Int Surf Coef						8.29	
Window	Double glazing unit	–	2500	–	750	1.06	3	–

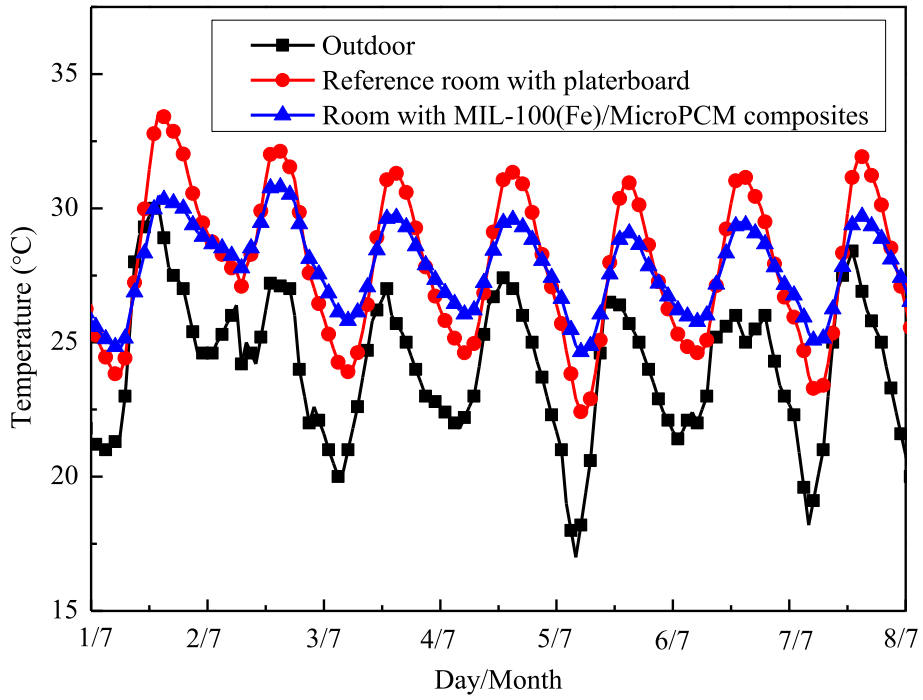

Fig. 11. Outdoor and simulated indoor temperature of reference room and room with MIL-100(Fe)/MicroPCM composites.

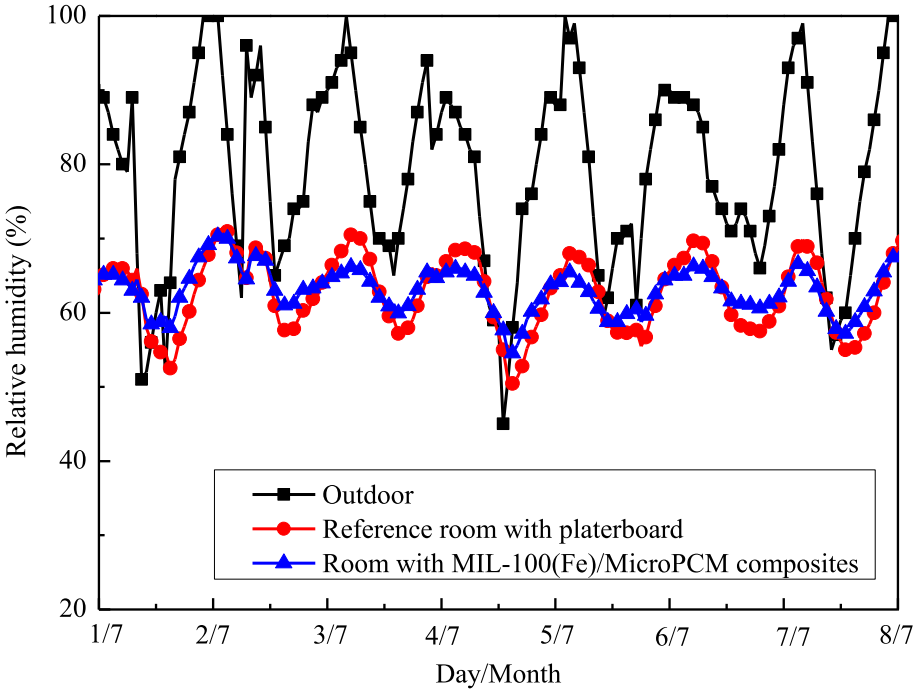

Fig. 12. Outdoor and simulated indoor relative humidity of reference room and room with MIL-100(Fe)/MicroPCM composites.

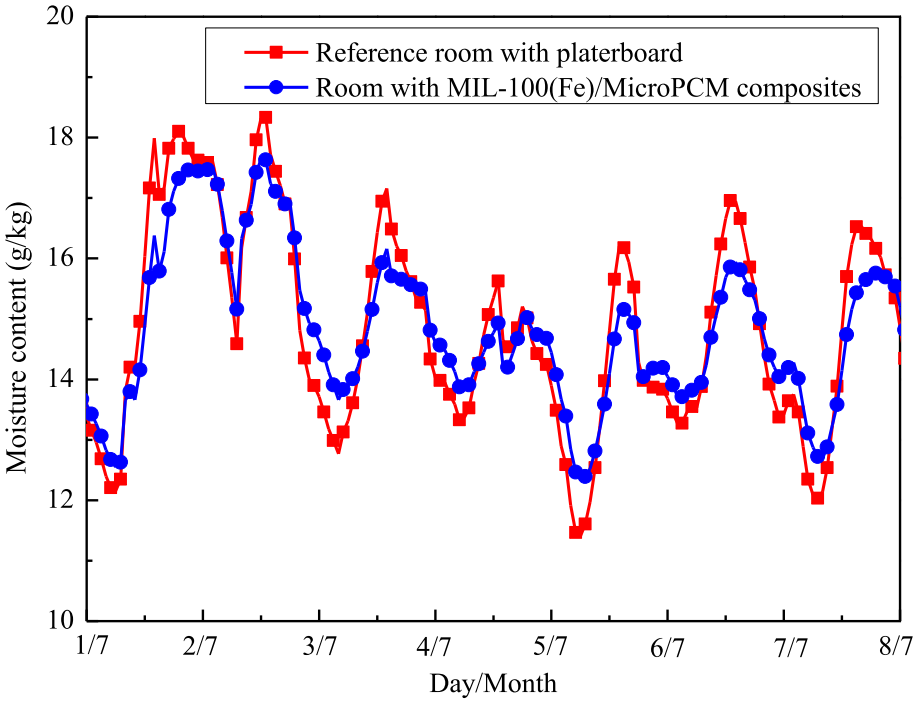

Fig. 13. Absolute humidity of reference room and room with MIL-100(Fe)/MicroPCM composites.

5. Conclusion

In this study, MicroPCM synthesized as thermal buffering material and MIL-(100) synthesized as humidity buffering material. A series of composites containing different proportions of MicroPCM and MIL-(100) were obtained by gridding two ingredients. The hygrothermal properties of the composites were characterized by experimental measurements. Hygrothermal buffering behavior of the composites containing 50% MicroPCM in a lightweight building was obtained by the simulation method. The results show as follows.

(1) When the content of MicroPCM in the composites is more than 50%, the trigger point of steep adsorption and desorption of MIL-100(Fe)/MicroPCM moved from 20% to 40% RH to 70% and 70% RH, respectively. That means composites are easier to be regenerated than pure MIL-100 (Fe), which will increase its application in passive buildings.

(2) There is no chemical reaction between the MicroPCM and MIL-100(Fe) by simple grinding. The addition of MIL-100(Fe) doesn't change the crystallization form of MicroPCM. The enthalpy decreased with the increase of MIL-100(Fe) in the composites. The temperature and humidity control ability of composites has a trade-off relationship.
(3) Numerical results show that the composites show excellent thermal and moisture buffering behavior. Compared with the same thickness of the plasterboard, the composites can significantly reduce the temperature and humidity fluctuations. Thus the comfort of the room with MicroPCM/MIL-100 (Fe) composites is improved.

Declaration of competing interest

The authors declare that they have no known competing financial interests or personal relationships that could have appeared to influence the work reported in this paper.

CRediT authorship contribution statement

Pumin Hou: Writing - original draft, Investigation. **Menghao Qin:** Conceptualization, Supervision. **Shuqing Cui:** Methodology. **Kan Zu:** Data curation.

Acknowledgements

The authors would like to thank the China Scholarship Council (CSC) for financially supporting Pumin Hou during his stay at the Technical University of Denmark (NO. 201803170122).

References

[1] A. Waqas, Z. Ud Din, Phase change material (PCM) storage for free cooling of buildings-A review, Renew. Sustain. Energy Rev. 18 (2013) 607–625.
[2] British Petroleum (B.P), Statistical Review of World Energy, 2010.
[3] E. Maleviti, W. Wehrmeyer, Y. Mulugetta, An empirical assessment to express the variability of buildings' energy consumption, Int. J. Energy Optim. Eng. 2 (3) (2013) 55–67.
[4] R. Yao, V. Costanzo, X. Li, et al., The effect of passive measures on thermal comfort and energy conservation. A case study of the hot summer and cold winter climate in the Yangtze River region, J. Build Eng. 15 (2018) 298–310.
[5] H. Akeiber, P. Nejat, M.Z.A. Majid, et al., A review on phase change material (PCM) for sustainable passive cooling in building envelopes, Renew. Sustain. Energy Rev. 60 (2016) 1470–1497.
[6] M. Song, F. Niu, N. Mao, et al., Review on building energy performance improvement using phase change materials[J], Energy Build. 158 (2018) 776–793.
[7] F. Kuznik, D. David, K. Johannes, et al., A review on phase change materials integrated in building walls[J], Renew. Sustain. Energy Rev. 15 (1) (2011) 379–391.
[8] M. Zhang, M. Qin, C. Rode, et al., Moisture buffering phenomenon and its impact on building energy consumption, Appl. Therm. Eng. 124 (2017) 337–345.
[9] A. Trabelsi, R. Belarbi, K. Abahri, M. Qin, Assessment of temperature gradient effects on moisture transfer through thermogradient coefficient, Build. Simulat. 5 (2) (2012) 107–115.
[10] R. El Diasty, P. Fazio, I. Budaiwi, Modelling of indoor air humidity: the dynamic behaviour within an enclosure, Energy Build. 19 (1) (1992) 61–73.
[11] Z. Chen, M. Qin, J. Yang, Synthesis and characteristics of hygroscopic phase change material: composite microencapsulated phase change material (MPCM) and diatomite, Energy Build. 106 (2015) 175–182.
[12] Z. Chen, M. Qin, Preparation and hygrothermal properties of composite phase change humidity control materials, Appl. Therm. Eng. 98 (2016) 1150–1157.
[13] Z. Chen, D. Su, M. Qin, et al., Preparation and characteristics of composite phase change material (CPCM) with SiO2 and diatomite as endothermal-hydroscopic material, Energy Build. 86 (2015) 1–6.
[14] Z. Wu, M. Qin, M. Zhang, Phase change humidity control material and its impact on building energy consumption, Energy Build. 174 (2018) 254–261.
[15] X. Feng, M. Qin, S. Cui, et al., Metal-organic framework MIL-100 (Fe) as a novel moisture buffer material for energy-efficient indoor humidity control, Build. Environ. 145 (2018) 234–242.
[16] X. Zheng, T.S. Ge, R.Z. Wang, Recent progress on desiccant materials for solid desiccant cooling systems, Energy 74 (2014) 280–294.
[17] G. Férey, C. Mellot-Draznieks, C. Serre, et al., A chromium terephthalate-based solid with unusually large pore volumes and surface area, Science 309 (5743) (2005) 2040–2042.
[18] O.M. Yaghi, M. O'Keeffe, N.W. Ockwig, et al., Reticular synthesis and the design of new materials, Nature 423 (6941) (2003) 705.
[19] O.M. Yaghi, M. O'keeffe, N.W. Ockwig, et al., Reticular synthesis and the design of new materials, Nature 423 (6941) (2003) 705.
[20] G. Férey, Hybrid porous solids: past, present, future, Chem. Soc. Rev. 37 (1) (2008) 191–214.
[21] S.M. Cohen, Modifying MOFs: new chemistry, new materials, Chem. Sci. 1 (1) (2010) 32–36.
[22] H. Furukawa, F. Gándara, Y.B. Zhang, et al., Water adsorption in porous metal–organic frameworks and related materials, J. Am. Chem. Soc. 136 (11) (2014) 4369–4381.
[23] P. Horcajada, S. Surblé, C. Serre, et al., Synthesis and catalytic properties of MIL-100 (Fe), an iron (III) carboxylate with large pores, Chem. Commun. (27) (2007) 2820–2822.
[24] Y.K. Seo, J.W. Yoon, J.S. Lee, et al., Large scale fluorine-free synthesis of hierarchically porous iron (III) trimesate MIL-100 (Fe) with a zeolite MTN topology, Microporous Mesoporous Mater. 157 (2012) 137–145.
[25] J. Shi, X. Wu, X. Fu, et al., Synthesis and thermal properties of a novel nanoencapsulated phase change material with PMMA and SiO2 as hybrid shell materials, Thermochim. Acta 617 (2015) 90–94.
[26] R. Canioni, C. Roch-Marchal, F. Sécheresse, et al., Stable polyoxometalate insertion within the mesoporous metal organic framework MIL-100 (Fe), J. Mater. Chem. 21 (4) (2011) 1226–1233.
[27] L. Han, H. Qi, D. Zhang, et al., A facile and green synthesis of MIL-100 (Fe) with high-yield and its catalytic performance, New J. Chem. 41 (22) (2017) 13504–13509.
[28] S.E. Moradi, S. Dadfarnia, A.M. Haji Shabani, et al., Removal of Congo red from aqueous solution by its sorption onto the metal organic framework MIL-100 (Fe): equilibrium, kinetic and thermodynamic studies, Desalination Water Treat. 56 (3) (2015) 709–721.
[29] J.W. Yoon, Y.K. Seo, Y.K. Hwang, et al., Controlled reducibility of a metal–organic framework with coordinatively unsaturated sites for preferential gas sorption, Angew. Chem. Int. Ed. 49 (34) (2010) 5949–5952.
[30] S. Huang, K.L. Yang, X.F. Liu, et al., MIL-100 (Fe)-catalyzed efficient conversion of hexoses to lactic acid, RSC Adv. 7 (10) (2017) 5621–5627.
[31] C. Alkan, A. Sarı, A. Karaipekli, Preparation, thermal properties and thermal reliability of microencapsulated n-eicosane as novel phase change material for thermal energy storage, Energy Convers. Manag. 52 (1) (2011) 687–692.
[32] A. Sarı, C. Alkan, A. Karaipekli, Preparation, characterization and thermal properties of PMMA/n-heptadecane microcapsules as novel solid–liquid microPCM for thermal energy storage, Appl. Energy 87 (5) (2010) 1529–1534.
[33] M. Qin, J. Yang, Evaluation of different thermal models in EnergyPlus for calculating moisture effects on building energy consumption in different climate conditions, Build. Simulat. 9 (2016) 15–25.
[34] R. Judkoff, J. Neymark, International Energy Agency Building Energy Simulation Test (BESTEST) and Diagnostic Method, National Renewable Energy Lab., 1995.